of catecholamines by the heart using PET. However, the interplay between metabolism and storage of ^{11}C-EPI in normal and specific disease conditions warrants further investigation.

ACKNOWLEDGMENTS

REFERENCES

1. Chierchia S, Davies G, Berkenboom G, Crea F, Crean P, Meseri A. Alphaadrenergic receptors and coronary spasm: an elusive link. *Circulation* 1984;69:8.
2. Watkins PJ, Mackay JD. Cardiac denervation in diabetic neuropathy. *Ann Intern Med* 1980;92:304–7.
3. Corr PB, Gillis RA. Autonomic neural influence on the dysrhythmias resulting from myocardial infarction. *Circ Res* 1978;43:1.
4. Lown B, Verrier RL, Rabinowitz SH. Neural and psychologic mechanisms and the problem of sudden death. *Am J Cardiol* 1977;39:890.
5. Lown B, Verrier RL. Neural activity and ventricular fibrillation. *N Engl J Med* 1976;294:1165.
6. Allman KC, Stevens MJ, Wieland DM, et al. Noninvasive assessment of cardiac diabetic neuropathy by carbon-11 hydroxyephedrine and positron emission tomography. *JACC* 1993;22:1425–1432.
7. Allman KC, Wieland DM, Muzik O, DeGrado TR, Wolfe ER, Schwaiger M. Carbon-11 hydroxyephedrine with positron emission tomography for serial assessment of cardiac adrenergic neuronal function after acute myocardial infarction in humans. *JACC* 1993;22:368–375.
8. Goldstein DS, Chang PC, Eisenhofer G, et al. Positron emission tomographic imaging of cardiac sympathetic innervation and function. *Circulation* 1990;81:1606–1621.
9. Schwaiger M, Guibourg H, Rosenspire K, et al. Effect of regional myocardial ischemia on sympathetic nervous system as assessed by fluorine-18-metaraminol. *J Nucl Med* 1990;31:1352–1357.
10. Schwaiger M, Kalff V, Rosenspire K, et al. Noninvasive evaluation of sympathetic nervous system in human heart by positron emission tomography. *Circulation* 1990;82:457–464.
11. Eisenhofer G, Hovevey-Sion D, Kopin IJ, et al. Neuronal uptake and metabolism of 2- and 6-fluorodopamine: false neurotransmitters and positron emission tomographic imaging of sympathetically innervated tissues. *J Pharmacol Exp Ther* 1989;248:419–429.
12. Fowler JS, Ansari AN, Atkins HL, et al. Synthesis and preliminary evaluation in animals of carrier-free ^{11}C-1-dopamine hydrochloride. *J Nucl Med* 1973;14:867–869.
13. Ding YS, Fowler JS, Gatley SJ, et al. Synthesis of high specific activity 6-[^{18}F]fluorodopamine for positron emission tomography studies of sympathetic nervous tissue. *J Med Chem* 1991;34:861–863.
14. Ding YS, Fowler JS, Gatley SJ, et al. Synthesis of high specific activity (+) and (−)-6-[^{18}F]fluoronorepinephrine via the nucleophilic aromatic substitution reaction. *J Med Chem* 1991;34:861–863.
15. Mislanka SG, Gildersleeve DL, Toorongian SA, et al. 6[^{18}F]fluoro-metaraminol: a radiotracer for in vivo mapping of adrenergic nerves of the heart. *J Med Chem* 1988;31:362–366.
16. Chakraborty PK, Gildersleeve DL, Toorongian SA, et al. Synthesis of [^{11}C]epinephrine and other biogenic amines by direct methylation of normethyl precursors. *J Lab Compd Radiopharm* 1992;32:172–173.
17. Wieland DM, Rosenspire KC, Hutchins GD, et al. Neuronal mapping of the heart with 6-[^{18}F]fluorometaraminol. *J Med Chem* 1990;33:956–964.
18. Rosenspire KC, Haka MS, Van Dort ME, et al. Synthesis and preliminary evaluation of carbon-11-meta-hydroxyephedrine: a false transmitter agent for heart neuronal imaging. *J Nucl Med* 1990;31:1328–1334.
19. Schwaiger M, Hutchins GD, Kalff V, et al. Evidence for regional catecholamine uptake and storage sites in the transplatned human heart by positron emission tomography. *J Clin Invest* 1991;87:1681–1690.
20. Wolpers HG, Nguyen N, Rosenspire KC, et al. Carbon-11-hydroxyephedrine as marker for neuronal marker for neuronal carecholamine retetion in reperfused canine myocardium. *Coron Artery Dis* 1991;2:923–929.
21. DeGrado TR, Hutchins GD, Toorongian SA, Wieland DM, Schwaiger M. Myocardial kinetics of carbon-11-metahydroxyephedrine: retention and effects of norepinephrine. *J Nucl Med* 1993;34:1287–93.
22. Iversen LL. The uptake of noradrenaline by the isolated perfused rat heart. *Br J Pharmacol* 1963;21:523–537.
23. Iversen LL. The uptake of adrenaline by the isolated perfused rat heart. *Br J Pharmacol* 1965;24:387–394.
24. Iversen LL. Inhibition of noradrenaline uptake by drugs. *J Pharm Pharmacol* 1965;17:62–64.
25. Iversen LL, Glowinski J, Axelrod J. The uptake and storage of ^{3}H-norepinephrine in the reserpine-pretreated rat heart. *J Pharm Exp Ther* 1965;150:173–183.
26. Eisenhofer G, Smolich J, Esler M. Disposition of endogenous adrenaline compared to noradrenaline relased by caridac sympathetic nerves in the anaesthetized dog. *Arch Pharmacol* 1992;345:160–171.
27. Taegtmeyer H, Hems R, Krebs HA. Utilization of energy-providing substrates in the isolated working rat heart. *Biochem J* 1980;186:701–711.
28. Wieland DM, Chakraborty PK, Gildersleeve DL, et al. Comparison of true and false neurotransmitters in the heart: evaluation of R-(−)-[^{11}C] epinephrine in animals [Abstract]. *J Nucl Med* 1993;34(suppl):123P.
29. DeGrado TR, Zalutsky MR, Vaidyanathan G. Uptake mechanisms of meta-iodobenzylguanidine uptake and retention in isolated rat heart. *Nucl Med Biol* 1995;22:1–12.

Comparison of Motion Correction Algorithms for Cardiac SPECT

W.D. Leslie, Jacqueline O. Dupont, Donna McDonald and Anne E. Peterdy

Department of Nuclear Medicine, St. Boniface General Hospital, University of Manitoba, Winnipeg, Canada

Patient motion remains a significant source of unsatisfactory cardiac SPECT examinations. The extent to which image recovery can be achieved with correction algorithms is unknown. **Methods:** Nine subjects who had completed motion-free redistribution ^{201}Tl cardiac SPECT subsequently underwent simultaneous dual-isotope (^{201}Tl/ ^{99m}Tc) SPECT with a ^{99m}Tc cutaneous point source, while the imaging table was subjected to predefined nonreturning y-translation movements. Cardiac reconstructions, marker reconstructions and marker-compressed dynamic images were generated from the raw data after applying the following correction methods: diverging squares, cross-correlation of the cardiac data and cross-correlation of the marker. **Results:** Marker cross-correlation performed significantly better than all other methods with good-excellent results in all evaluations. This compared with good-excellent results in none of 27 for the raw data, in 13 of 27 for cardiac cross-correlation and in 7 of 27 for diverging squares (p < 10^{-5}). The superiority of the marker-based method was confirmed on analysis of bullseye difference maps and quantitation of residual motion in the point-source data. **Conclusion:** Motion artifacts can accurately be detected and corrected using cross-correlation of an external point-source. Furthermore, this technique provides useful independent information on the degree of image recovery.

Key Words: thallium-201; SPECT; motion artifacts; myocardial perfusion

Patient motion can seriously degrade clinical SPECT imaging, and motion effect has been particularly well studied in relation to myocardial perfusion scintigraphy (*1–4*). Although many algorithms have been proposed for the identification of cardiac motion, some of these are strictly visual while others require operator intervention for motion correction. While the use of a cutaneous point-source has been advocated for the qualitative

assessment of motion and for manual image realignment, this method has not been widely used for automated correction (5). The most commonly used quantitative techniques use image cross correlation (6) or diverging squares (7) algorithms. Although both methods have been quite successful in data recovery using simulated motion in phantoms and patients, this underestimates the complexity of clinical motion that does not coincide with frame advances and does not consist of integral pixel shifts. Clinical validation of a data recovery algorithm requires that motion-corrected images be compared with a gold standard motion-free study under typical clinical conditions.

We became interested in the use of dual-isotope SPECT with one acquisition window used to acquire the ^{201}Tl cardiac data and a second used to acquire data on a cutaneous ^{99m}Tc point-source. This approach has the advantage of producing a highly detailed record of patient motion in the ^{99m}Tc window but does not affect the ^{201}Tl dataset. An investigation was undertaken to directly compare the clinical performance of three motion recovery tools: cross correlation, diverging squares and dual-isotope SPECT with a fiducial marker.

MATERIALS AND METHODS

Subjects

Nine subjects agreed to participate in the study (7 men, 2 women, mean age of 63 ± 13 yr). All subjects had been referred to the nuclear medicine laboratory for assessment and/or localization of myocardial ischemia. Two patients had a history of previous infarction and two had previously undergone coronary artery bypass grafting.

Data Acquisition

Each patient underwent standard stress-redistribution ^{201}Tl cardiac SPECT imaging. Symptom-limited treadmill exercise was performed with injection of 90 MBq (2.5 mCi) ^{201}Tl at peak exercise. Exercise was continued for 1 min postinjection. Imaging began approximately 10 min postinjection and was performed on a single-detector rotating gamma camera using 30 step-and-shoot projections of 20 sec each from the RAO to the LPO positions. A high-resolution, low-energy collimator was used. Imaging was repeated 3–4 hr later using the identical acquisition parameters. Three of the nine subjects had received an additional resting reinjection of 37 MBq (1.0 mCi) ^{201}Tl. Observation of the patient during the acquisition and inspection of the raw redistribution data on rotating cine display confirmed that the redistribution study was motion-free. The patient immediately underwent a second data acquisition using dual-isotope ^{201}Tl/^{99m}Tc SPECT after placing a low-activity (0.1–0.5 MBq) ^{99m}Tc marker in the left midclavicular line. The acquisition parameters were kept constant. The patient was subjected to a variable number of nonreturning vertical (y-axis) translation motions during the course of the acquisition that were achieved by manually moving the imaging table in a predefined manner. The number of discrete movements (range 2–6), direction (cranial or caudad), magnitude (small = 1 cm, medium = 2 cm, large = 3 cm) and timing (seconds into the acquisition) were determined with a pseudorandom number generator. Table 1 outlines the specific motion applied to each patient study.

Image Processing

Each pair of ^{201}Tl (cardiac) and ^{99m}Tc (marker) motion SPECT studies was subjected to motion detection and correction according to the three following methods.

Cardiac Cross-Correlation (Method 1). The algorithm of Eisner et al. (6) was programmed as outlined in the reference. We included subtraction of a constant level of background from the cardiac projection data as this has been shown to improve tracking

TABLE 1
Number, Direction, Magnitude and Timing of Movements Applied

Patient no.	Age (yr)	Sex	Movements
1	69	M	U2(181); U3(417); D1(663); D2(728); U2(769)
2	36	M	U3(104); D2(252); D2(536)
3	56	M	D2(464); U3(961)
4	67	M	U3(348); U3(830)
5	68	M	D3(106); U2(450)
6	40	F	D3(243); U2(374); U2(989)
7	60	M	D3(347); U2(453); U3(698); D1(988)
8	79	F	U2(110); D2(182); U1(453); D3(856); U1(1002)
9	71	M	D2(243); U3(436); D3(546)

Each movement is coded as direction (U = up, D = down), magnitude (cm) followed by timing (seconds into acquisition) are in parentheses.

of cardiac motion when there is a low signal-to-background ratio. Cardiac cross-correlation was performed across a range of background subtraction levels in order to determine the optimal value. When there is insufficient background subtraction then additional subtraction increases the amplitude of the motion histogram, but at a given level this stabilizes. The optimal subtraction value was taken as the point where the motion histogram stabilized. The motion histogram, so defined, was then applied to both the cardiac and marker datasets to produce motion-corrected studies, using interpolation to approximate subpixel correction. The threshold for motion correction was 0.4 pixels.

Diverging Squares (Method 2). The algorithm was implemented according to the method of Geckle et al. (7) and was applied to the cardiac dataset. Motion correction of the cardiac and point-source datasets was performed as described in Method 1.

Marker Cross-Correlation (Method 3). The motion histogram was derived from the marker image data using the same cross-correlation technique as in Method 1. Motion correction of the cardiac and marker data was then performed as described in Method 1. Four variations of the marker-based algorithm were compared by varying the reference frame for realignment (frame 1 for cumulative, adjacent frame for differential) and the degree of correction (subpixel or integral). For purposes of comparison with Methods 1 and 2, marker cross-correlation refers to the variation using cumulative motion detection with subpixel correction.

Image Analysis

The motion-correction algorithms provided seven pairs of cardiac-marker SPECT data per patient (including the initial uncorrected data). The cardiac and marker datasets were reconstructed using standard filtered backprojection techniques with a Hanning filter and no attenuation correction. Image displays were generated for the cardiac data that presented corresponding short-axis, vertical long-axis and horizontal long-axis slices from the motion-free and motion-corrected data. Additional displays for the reconstructed markers and marker compressed dynamic images (CDI) were created from the uncorrected and motion-corrected marker data. The marker CDI is a functional image that depicts the temporal aspects of y-axis motion. It is created by juxtaposing vertical columns of pixels from each data frame such that each column passes through the count center of the marker, and is analogous to the widely used technique for assessing esophageal motility. Deviation upwards or downwards from a horizontal track indicates upwards or downwards longitudinal motion of the patient. All displays were stored in random order without any information to identify the presence/absence of motion or mode of correction.

Two reviewers who were blinded to the study were asked to review the unlabeled random-ordered displays of cardiac recon-

structions, marker reconstructions and marker CDIs. The cardiac reconstructions were judged by how closely the motion-corrected study approximated the motion-free images, and were graded as excellent, good, fair or poor (where excellent and good studies were considered suitable for clinical interpretation while fair and poor studies were not and would have led to clinical misinterpretation). The marker reconstructions and CDIs were graded by the degree to which the images approximated a circular point source or a smooth horizontal line, respectively.

The amount of image distortion in the postcorrection data was measured objectively using bullseye maps of the cardiac reconstruction images and quantification of residual motion in the point source projection data. All pixels in the motion-free and motion-corrected bullseye maps were compared with a low-risk reference group and flagged as normal or abnormal using 2 s.d. below the reference mean as the cutoff. The number of pixels that were discordant between the two maps was designated the bullseye difference index (BDI). The BDI correlated well with the visual gradings of the cardiac reconstructions ($p < 10^{-5}$), marker reconstructions ($p = 0.003$) and marker CDIs ($p = 0.01$). After application of the correction algorithms, the amount of residual patient motion was also calculated from the motion-corrected marker studies. First, an integral motion histogram, $H(i)$, was derived by reapplying Method 3 (cumulative-subpixel) to the marker study. Pixel shift scores were then computed as:

$$\text{Pixel shift score (PSS)} = \sum_i |H(i) - H|.$$

Prigent et al. (2) have shown that a similarly defined index correlates with motion artifacts. We also found that PSS correlated well with the visual gradings of the cardiac reconstructions ($p < 10^{-6}$), marker reconstructions ($p < 10^{-18}$) and marker CDIs ($p < 10^{-19}$).

Statistical Analysis

All analysis was performed with CSS:Statistica V3.0a (Statsoft Inc., Tulsa, OK). Image grades were compared using nonparametric techniques. Paired data was assessed with the Wilcoxon matched pairs test while multiple groups were compared using Kruskal-Wallis analysis of variance. Correlation between variables was assessed with the Kendall-Tau correlation coefficient. Chi-square analysis (comparison of multiple methods) or Fisher's exact test (comparison of two methods) was used to assess frequency of acceptable (good-excellent) and unacceptable (fair-poor) grades. A $p < 0.05$ was taken to indicate a statistically significant difference or association. Ranges are expressed as mean ± s.e.

RESULTS

Visual Assessment

Each of the motion-correction algorithms resulted in a statistically significant improvement in the gradings whether this was based on the cardiac reconstruction, marker reconstruction or marker CDI (Fig. 1). Visual assessment of the corrected cine projection data revealed a small amount of residual motion in two cases after application of cardiac cross-correlation (Method 1), three cases of unacceptable motion after diverging squares (Method 2) but no appreciable residual motion after the marker-based correction (Method 3). There were highly significant between-methods differences in the image gradings for the uncorrected, cardiac cross-correlation, diverging squares and marker cross-correlation datasets, and again this was evident in both the cardiac reconstruction ($p = 0.0001$), marker reconstruction ($p < 0.0001$) and marker CDI image ($p < 0.0001$). There was a slight trend in favor of cardiac cross-correlation over diverging squares, but this was not statistically significant.
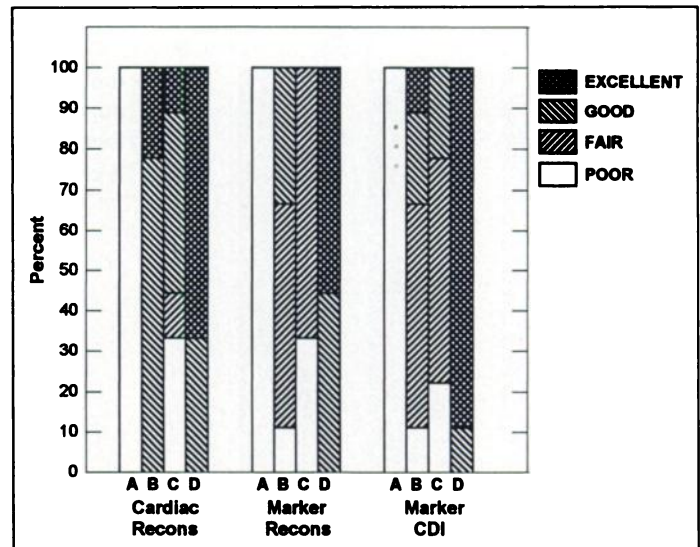

FIGURE 1. Comparative visual gradings for the cardiac reconstruction, marker reconstruction and marker CDI from the following correction algorithms: A = uncorrected, B = cardiac cross-correlation, C = diverging squares, D = marker cross-correlation (using cumulative detection and subpixel correction).

Marker cross-correlation performed better than either cardiac cross-correlation (cardiac reconstruction, $p = 0.07$; marker reconstruction, $p = 0.01$; marker CDI, $p = 0.01$) or diverging squares (cardiac reconstruction, $p = 0.07$; marker reconstruction, $p < 0.01$; marker CDI, $p < 0.01$).

A global measure of the performance of each algorithm was computed as the total number of displays (cardiac reconstruction, marker reconstruction and marker CDI) that were judged to be of acceptable clinical quality (grade good or excellent, maximum score 27). The uncorrected data scored 0, cardiac cross-correlation scored 13, diverging squares scored 7 and marker cross-correlation scored 27. These differences were highly significant, both clinically and statistically (chi square 33.6 df 3, $p < 10^{-5}$).

In a second analysis, the four modifications of marker cross-correlation (Method 3) were compared to one another. Not surprisingly, differences were much less striking. No significant difference was seen in the gradings for the cardiac reconstructions. The marker reconstructions and CDI images did show statistically significant differences ($p = 0.05$ and $p = 0.0002$, respectively), and these favored the method that used cumulative motion detection with subpixel correction (Fig. 2).

In many cases, the reviewers found the differences between the cardiac reconstructions quite subtle whereas the marker-based methods proved much easier to judge. The marker-based gradings also correlated strongly with cardiac reconstruction gradings (Kendel-Tau $p < 10^{-8}$ compared with marker reconstruction and $p < 10^{-8}$ compared with marker CDI). Thus, it appeared that the point source-based methods provided independent validation of the degree of data recovery and clinical utility of the postcorrection cardiac data.

Quantitative Measures

Quantification of the residual motion artifact in the bullseye maps gave results that paralleled the visual assessment. The mean BDI decreased from 3468 ± 666 in the uncorrected study to 2226 ± 455 for cardiac cross-correlation, 2713 ± 624 for diverging squares and 1747 ± 537 for marker cross-correlation (ANOVA $p = 0.09$).

Improvement in the pixel shift score (PSS) correlated closely with the visual gradings (Fig. 3). The mean PSS decreased from
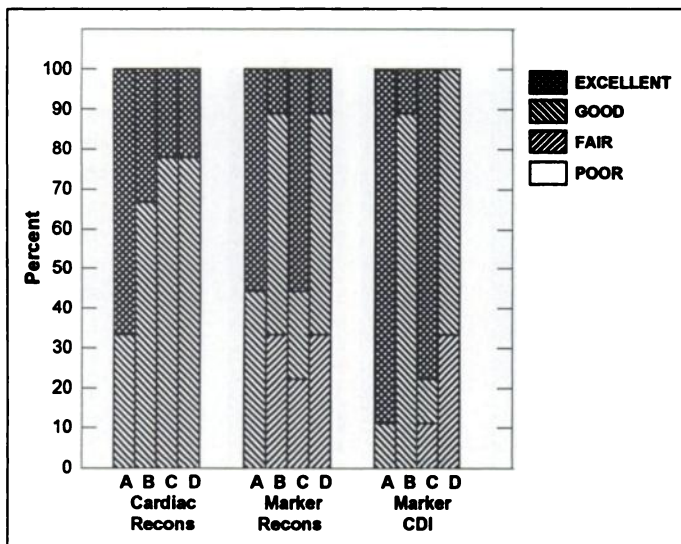
FIGURE 2. Comparative visual gradings for the cardiac reconstruction, marker reconstruction and marker CDI from the variations of the marker cross-correlation algorithm. A = cumulative-subpixel, B = cumulative-integral, C = differential-subpixel, D = differential-integral.

40.4 ± 2.6 in the uncorrected study to 15.4 ± 1.8 for cardiac cross-correlation, 26.7 ± 3.6 for diverging squares and 1.7 ± 0.2 for marker cross-correlation (ANOVA $p < 0.0001$). The mean PSS for marker cross-correlation was significantly less than that for cardiac cross-correlation ($p = 0.0003$) or diverging squares ($p = 0.0003$). Cardiac cross-correlation gave lower mean PSS than diverging squares ($p = 0.007$) while the latter in turn was significantly less than for the uncorrected data ($p < 0.02$). The cumulative-subpixel variation on the marker-based method (PSS 1.7 ± 0.2) performed better (ANOVA $p = 0.0003$) than cumulative-integral (6.1 ± 0.3), differential-subpixel (6.4 ± 3.0) and differential-integral (10.6 ± 2.6). PSS was significantly greater when cardiac image quality was graded as unsatisfactory (fair-poor) as compared with a satisfactory (good-excellent) grade: 35.4 ± 11.0 (s.d.) versus 7.9 ± 8.2, respectively ($p < 10^{-15}$). PSS accurately predicted a
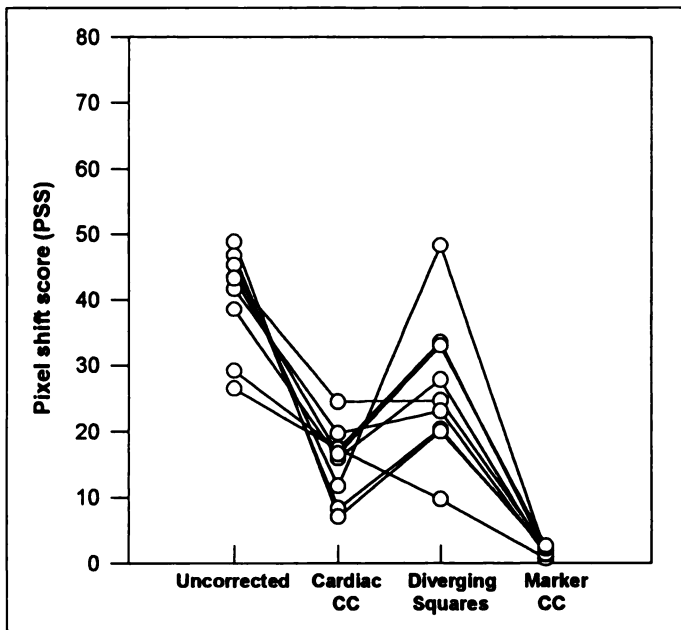

FIGURE 3. PSS calculated from the ^{99m}Tc cutaneous point source before and after motion correction using cardiac cross-correlation, diverging squares and marker cross-correlation; $p \leq 0.0003$ for all comparisons with marker cross-correlation.
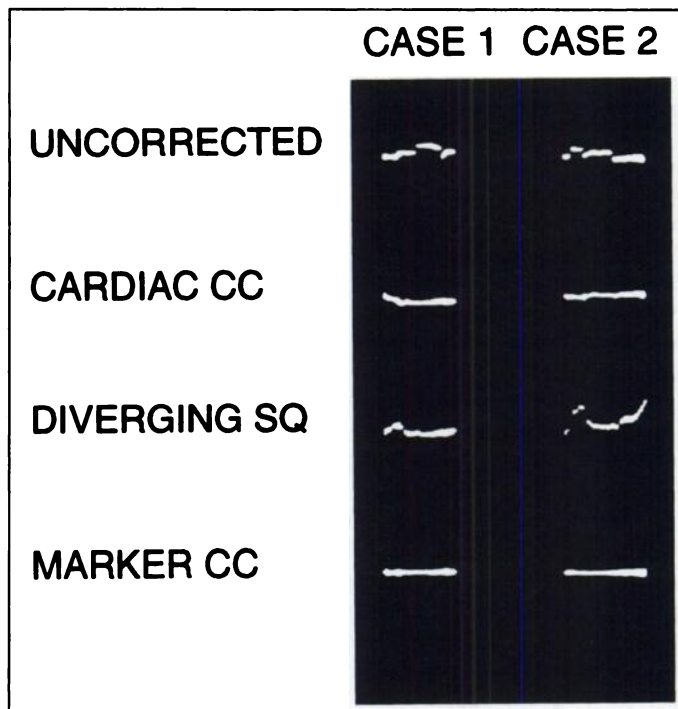

FIGURE 4. Marker CDI displays for Case 1 and Case 2. Deviations from a linear track are present in the uncorrected, cardiac cross-correlation (cardiac CC) and diverging squares (diverging SQ), while a linear track is obtained with marker cross-correlation (marker CC).

satisfactory (good-excellent) grade for cardiac reconstruction: a value less than 21 gave satisfactory images in 50 of 52 (98%) whereas a value greater than 21 gave unsatisfactory images in 13 of 20 (65%).

Case Examples

Figure 4 presents the marker CDIs for two subjects. There are stepwise shifts in the uncorrected marker tracks corresponding to each nonreturning vertical motion. Marker cross-correlation is successful at recovering a linear track while nonlinearities are present with the other methods. Diverging squares actually leads to a deterioration in the CDI for the second example due to erroneous tracking of the heart. The reconstructed cardiac images for Subject 2 demonstrate the effects of uncorrected motion (Fig. 5). The motion-free images show only a mild reduction in uptake by the anterolateral segment of the left ventricle. Uncorrected motion results in severe widespread artifacts and images that are clinically unacceptable. Good data recovery are achieved with the marker cross-correlation algorithm. The cardiac cross-correlation images are probably clinically acceptable despite a residual focal reduction in the inferior wall, but data recovery with diverging squares was unsatisfactory. The discrepancy between the motion-free and motion-corrected bullseye maps is least with marker cross-correlation (Fig. 6). This corresponded to a BDI of 3787 pixels for uncorrected motion, 2017 with cardiac cross-correlation, 5255 with diverging squares and 1141 with marker cross-correlation.

DISCUSSION

We have demonstrated that there are considerable differences in the clinical performance of motion-correction algorithms when these are applied to actual, rather than simulated, patient motion. The fact that each of these methods has performed well in simulated motion tests may reflect the fact that such evaluations often are done using simulated data with integral frame shifts and are, therefore, perfectly recoverable whereas clinical motion always entails some loss of resolution through
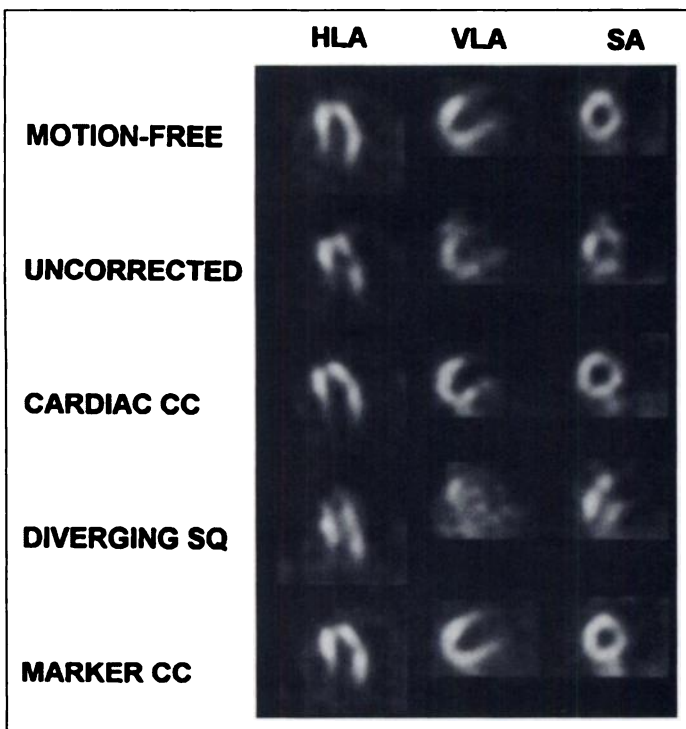
FIGURE 5. Thallium-201 cardiac reconstruction for Subject 2. The subject had been subjected to three nonreturning motions. The horizontal rows show the motion-free reference images, uncorrected data and the results from cardiac cross-correlation (cardiac CC), diverging squares (diverging SQ) and marker cross-correlation (marker CC). Cardiac cross-correlation recovers images that are very close to the reference images, while artifactual defects persist in all other image sets. Vertical long-axis, horizontal long-axis and short-axis projections.

subpixel and within-frame blurring. This is supported by the observation that even pure vertical motion encountered in clinical studies is difficult to correct (*4*). Despite these theoretical limits, however, we have shown that clinically usable data can be recovered with an external point-source method.

Although an effort was made to simulate patient motion as it occurs clinically, our experiment is by definition artificial. We only addressed translation of the patient using nonreturning
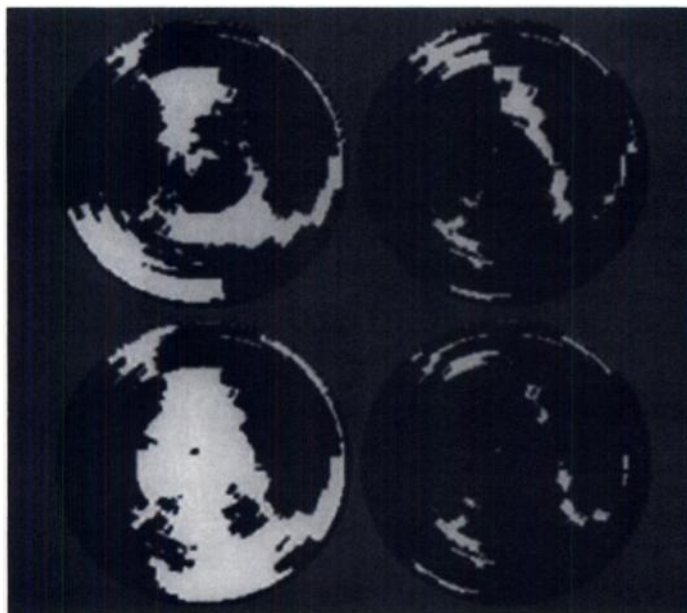

FIGURE 6. Thallium-201 bull's-eye difference maps for Subject 2 calculated for uncorrected motion (upper left), cardiac cross-correlation (upper right), diverging squares (bottom left) and marker cross-correlation (bottom right).

vertical (y-axis) translation. In a study of simulated cardiac motion, Cooper et al. (*8*) showed that vertical motion produced more artifacts than lateral motion. Our algorithm has not been validated for horizontal (x-axis) translation and would not be applicable to rotational motion, an important point since patient motion frequently cannot be explained by pure translation of the heart (*9*). It should be clearly stated that patient motion is not the only source of cardiac motion, since respiratory artifact and upward creep of the heart (*10*) represent cardiac motion relative to the rest of the patient and would not be detected with this method. On the other hand, organ-tracking procedures can introduce motion artifacts from breast attenuation or when there is significant nontarget background activity. At the present time, it is unclear which types of motion contribute most frequently and most severely to a deterioration in clinical image quality. For this reason, it is probably useful to have several methods available that can be applied to the appropriate situation, either singly or sequentially. Our experiment addressed motion with cardiac ^{201}Tl SPECT and may not be applicable to ^{99m}Tc-sestamibi. Although it would be a relatively simple matter to select a non-technetium isotope for the point source and adapt our method accordingly, the higher photon flux, higher filter cutoff and improved image quality associated with technetium-based cardiac perfusion agents may make these studies more sensitive to motion. We have observed that the high levels of subdiaphragmatic activity seen with ^{99m}Tc-sestamibi are particularly problematic for organ-tracking methods such as cross-correlation and diverging squares.

There have been very few attempts to compare several motion correction algorithms simultaneously. In a simulated study of vertical and lateral cardiac motion by Cooper et al. (*11*), the sensitivity of visually inspecting the cine data, cross-correlation, diverging squares and a technique called two-dimensional fitting were compared. They concluded that cine review, cross-correlation and two-dimensional fitting were more sensitive than diverging squares. The effect of the residual uncorrected motion on the cardiac images was not determined, however. Other investigators have described the use of fiducial markers, but their methods differ significantly from our own. Friedman et al. (*4*) described the use of a ^{57}Co cutaneous point source but depended on a visual assessment of motion from the summed image and integral pixel shifts to achieve visual realignment. Germano et al. (*12*) have developed a technique for multidetector cameras that is able to quantify translational vertical and lateral motion to submillimeter accuracy in phantom experiments. Unfortunately, they did not compare their method with either cross-correlation or diverging squares, and included only two clinical cases (neither of which involved ^{201}Tl). Our study used image quality to compare the effectiveness of several motion-comparison procedures simultaneously. Visual assessment of a cine display of the corrected projection data, although an important and necessary condition for adequate data recovery, did not appear to be sufficient to guarantee satisfactory image quality. We did verify that the pixel shift score, an easily obtained quantitative index derived from the marker data, accurately predicts adequate motion recovery using the same cutoff value proposed by Prigent et al. (*2*).

CONCLUSION

External marker cross-correlation can provide accurate data recovery of translational cardiac motion in the vertical axis. Furthermore, this method provides independent validation that accurate data recovery has been achieved. Future development and refinement of motion-correction algorithms should use

clinical test conditions since these appear to be more exacting than simulated motion.

REFERENCES

1. Eisner R, Churchwell A, Noever T, et al. Quantitative analysis of the tomographic thallium-201 myocardial bull's-eye display: critical role of correction for patient motion. *J Nucl Med* 1988;29:21-97.
2. Prigent FM, Hyun M, Berman DS, Rozanski A. Effect of motion on thallium-201 SPECT studies: a simulation and clinical study. *J Nucl Med* 1993;34:1845-1850.
3. Parker JA. Effect of motion on cardiac SPECT imaging [Editorial]. *J Nucl Med* 1993;34:1355-1356.
4. Botvinick EH, Zhu YY, O'Connell WJ, Dae MW. A quantitative assessment of patient motion and its effect on myocardial perfusion SPECT images. *J Nucl Med* 1993;34: 303-310.
5. Friedman J, Daniel MD, Berman S, et al. Patient motion in thallium-201 myocardial SPECT imaging an easily identified frequent source of artifactual defect. *Clin Nucl Med* 1988;13:321-324.
6. Eisner RL, Noever T, Nowak D, et al. Use of cross-correlation function to detect patient motion during SPECT imaging. *J Nucl Med* 1987;28:97-101.
7. Geckle WJ, Frank TL, Links JM, Becker LC. Correction for patient and organ movement in SPECT: application to exercise thallium-201 cardiac imaging. *J Nucl Med* 1988;29:441-450.
8. Cooper JA, Neumann PH, McCandless BK. Effect of patient motion on tomographic myocardial perfusion imaging. *J Nucl Med* 1992;33:1566-1571.
9. Eisner RL, Aaron AM, Worthy MR, et al. Apparent change in cardiac geometry during single-photon emission tomography thallium-201 acquisition: a complex phenomenon. *Eur J Nucl Med* 1993;20:324-329.
10. Friedman J, Van Train K, Maddahi J, et al. "Upward creep" of the heart: a frequent source of false-positive reversible defects during thallium-201 stress-redistribution SPECT. *J Nucl Med* 1989;30:1718-1722.
11. Cooper JA, Neumann PH, McCandless K. Detection of patient motion during tomographic myocardial perfusion imaging. *J Nucl Med* 1993;34:1341-1348.
12. Germano G, Chua T, Kavanagh B, Kiat H, Berman DS. Detection and correction of patient motion in dynamic and static myocardial SPECT using a multi-detector camera. *J Nucl Med* 1993;34:1349-1355.

FIRST IMPRESSIONS
Sudden Onset of Pain

Figure 1.

Figure 2.

PURPOSE

A 46-yr-old federal prison inmate experienced sudden onset of pain in his right proximal mid-thigh while walking across the prison yard. The patient had no significant past medical history. Radiographs of the right femur revealed a transverse fracture of the femoral shaft and abnormal thickening of the cortical bone with sclerosis of the trabeculae (Fig. 1). Laboratory results revealed elevated alkaline phosphatase at 165 IU/liter (30-115 nl) and normal serum calcium.

The patient was placed in skeletal traction and taken to the nuclear medicine department for a bone scan. Figure 2 reveals a fracture of the right femur and intense uptake in the right femur. No other abnormalities were noted on the whole-body scan. This transverse or "chalkstick" fracture was caused by Paget's disease of bone involving only the right femur. Paget's disease usually involves more than one bone (polyostotic), but it can be monostotic in 15%-30% of affected patients. Chalkstick fractures can also be seen in patients with fibrous dysplasia and osteomalacia.

The pathology report of the bone biopsy of the right femur also correlated with Paget's disease.

TRACER
Technetium-99m-HDP, 20 mCi

ROUTE OF ADMINISTRATION
Intravenous injection

TIME AFTER INJECTION
3 hours

INSTRUMENTATION
Siemens Diacam

CONTRIBUTORS
Rozina Maredia, DO and Kenneth J. Simcic, MD, William Beaumont Army Medical Center, El Paso, Texas